Supporting on-line material

Large scale growth and characterization of atomic hexagonal boron nitride layers

Li Song[†], Lijie Ci[†], Hao Lu[†], Pavel B. Sorokin[†], Chuanhong Jin[‡], Jie Ni[†], Alexander G. Kvashnin[§], Dmitry G. Kvashnin[§], Jun Lou[†], Boris, I. Yakobson[†], Pulickel M. Ajayan[†,*]

† Department of Mechanical Engineering & Materials Science, Rice University, Houston, TX 77005, USA

‡ Nanotube Research Center, National Institute of Advanced Industrial Science and Technology (AIST), Tsukuba 305-8565, Japan

§ Siberian Federal University, 79 Svobodny av., Krasnoyarsk, 660041, Russia

* To whom correspondence should be addressed. Tel: 1-713-3485904, Fax:1-713-3485423, Email: ajayan@rice.edu

1. Elemental mapping by Transmission Electron Microscopy:

With energy filtered imaging technique (GIF), we mapped the elemental distribution of B, N and C in a selected area of as-grown *h*-BN films. Figure S1a shows an edge TEM image of the film. Figure S1b and S1c present the elemental distribution of B and N in the selected image region of Fig. S1a. It is clear shown that B and N are uniformly distributed over the entire film. Carbon signals are not notable in the mapping. The mappings reveal that the film consists of B and N compound, which is distinct from our previous BNC domains.[1]

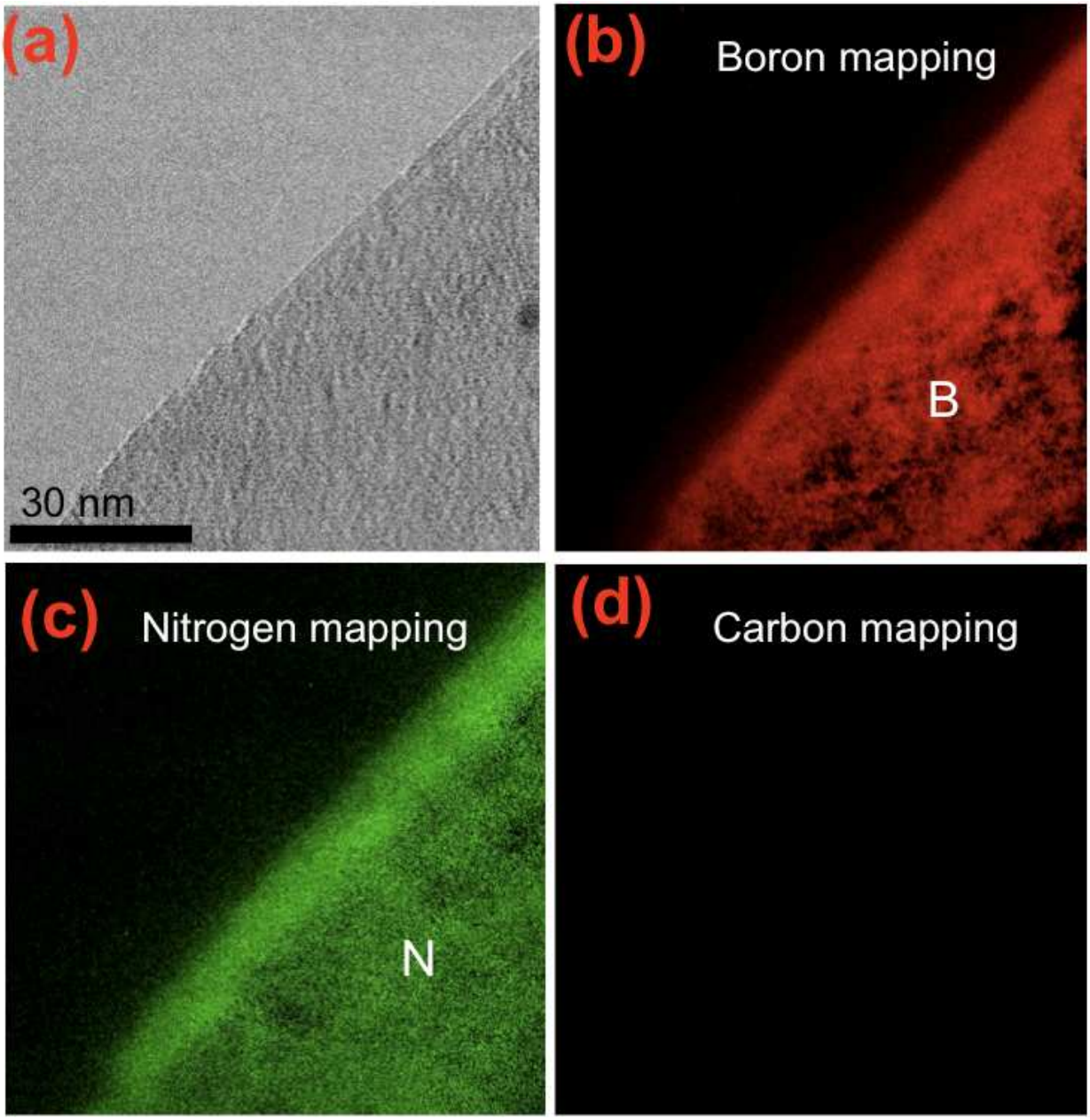

Figure S1: (a), Zero-loss TEM image of as-grown *h*-BN film. (b) and (c), GIF imaging show elemental distribution of boron and nitrogen, respectively. This indicates B and N are uniformly distribute over the entire selected area of the film. (d), Elemental mapping of carbon, indicating that carbon is not notable in the film by GIF imaging.

2. Electrical measurement:

To measure the electrical properties of these ultrathin BN films, standard lithography techniques were used to fabricate micron size devices with the channel length of 20-30 μm. Figure S2a shows the typical source-drain current vs. the source-drain voltage curves for several BN devices. It clear indicates that our as-grown BN sheets are good insulating materials. A typical device fabricated on *h*-BN film was shown in Fig. S2b.

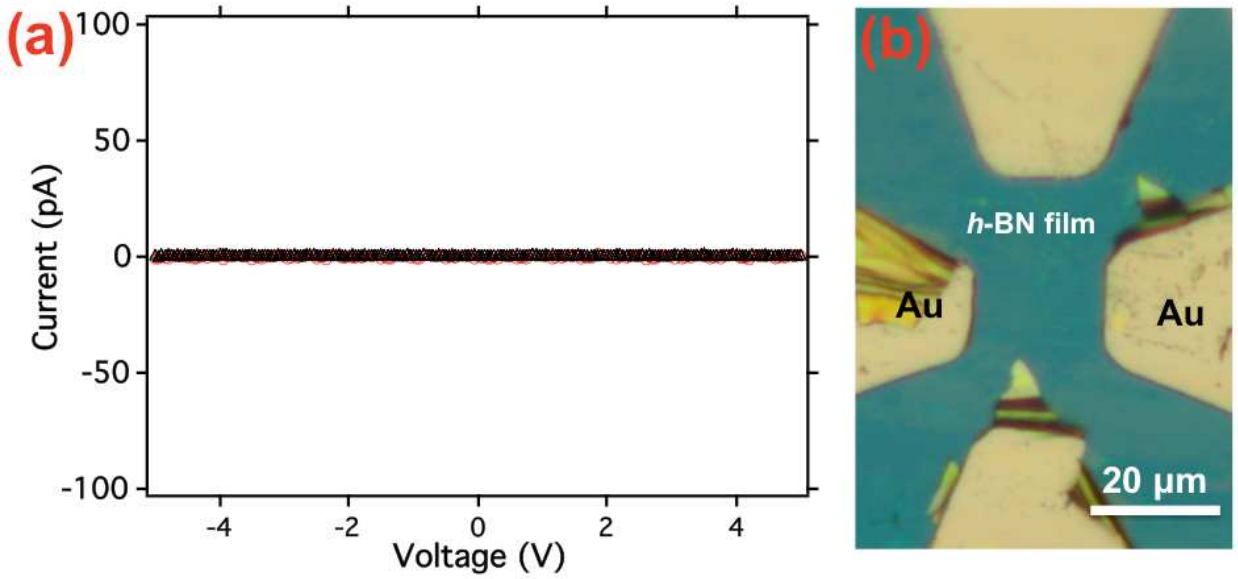

Figure S2: (a), Two typical I_{ds}-V_{ds} characteristics for *h*-BN film devices, indicating good insulating behavior of these as-grown films. (b) Optical microscopy image of the tested *h*-BN device with four gold electrodes, fabricated by photolithography technique.

3. Indentation measurements by Atomic force Microscopy:

The *h*-BN film was transferred onto pre-patterned holes substrates, as shown in Figure S3a. Compare with Area II region, area I region of Fig. S3a shows a series of freestanding *h*-BN membranes deposited over many circular wells with diameter 1 μm. Prior to indenting measurement, the suspended *h*-BN membranes were scanned in a noncontact AFM mode. A noncontact AFM image in Fig. S3b indicates that the suspended membranes were stretched across the holes. The height profile (marked as the dashed line) shows along the height at the edge of the membrane is about 20-50 nm, which indicates the membranes sinking down due to the van der Walls attraction from the bottom substrate and surface tension during film drying in our transferring process.

Mechanical testing was performed at a constant displacement rate and displacement controlled indentation, followed by load reversal. Once the data for elastic properties of the films were recorded, the films were once again indented at the same rate, but this time to failure. The force-displacement data were processed to determine the elastic properties and breaking stress of the *h*-BN membranes. A SEM image of a fractured membrane after indentation measurement is shown in Fig. S3c. This proves that our indenting measurement was probed at the center of suspended membranes. Figure S3d shows a SEM image of AFM tip after piercing into the suspended membrane. The flakes at the end of the tip are *h*-BN pieces from a broken membrane.

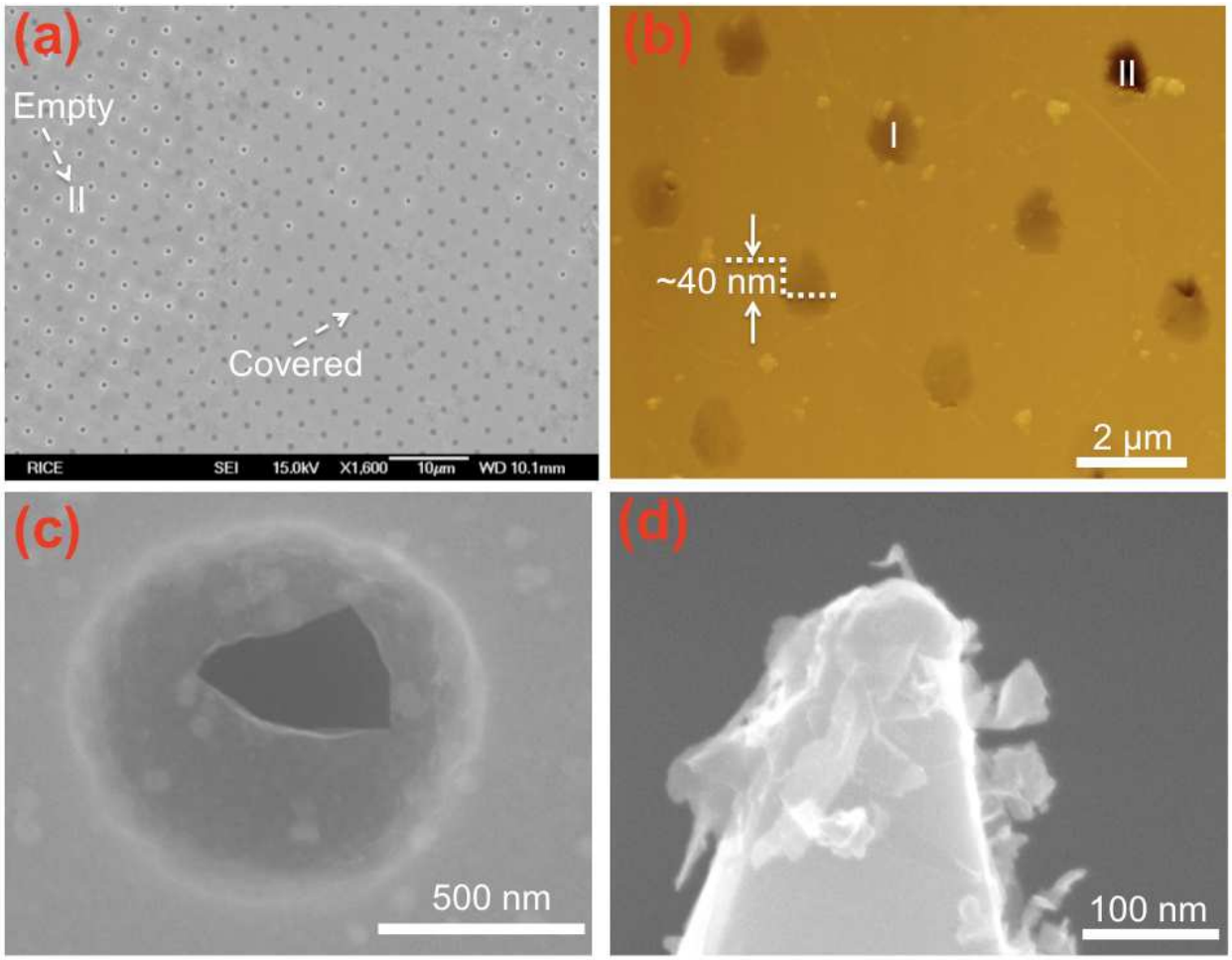

Figure S3: (a) Low magnification SEM image of a large *h*-BN film spanning an array of circular holes 1μm in diameter. Area I shows holes fully covered by film, area II shows fractured member region. (b) Noncontact mode AFM image of suspended membranes. The height profile (dashed line) shows along the height at the edge of the membrane is about 20-50 nm. (c), SEM image of a fractured membrane. (d) SEM image of AFM tip after indentation. The flakes at the end of the tip are *h*-BN pieces from a broken membrane.

4. Theoretical modeling:

To better understand the above indention experiment on BN film, we performed a molecular mechanics study of elastic properties of single BN layer, as well as BN sheet with various vacancy defects concentrations, as shown in Fig S4. The cone of the frozen atoms (imitating the atomic-force microscope tip) strains the BN membrane with frozen edges up to destruction. For the computation model we chose the BN sheet with diameter 14.8 nm and tip with diameter 1.63 nm. The atomic interactions were modeled by the Tersoff many-body potential.[2] In the Ref. 3 the parameterization for BN nanotubes was proposed. We fitted this parameterization for better reproducing the hexagonal BN structure and elastic properties. Parameters are shown in the Table S1 (notations correspond to Ref. 3).

Supplementary Table S1. The parameters for BN.

A (eV)	B (eV)	λ_1 (Å^{-1})	λ_2 (Å^{-1})	λ_3 (Å^{-1})	R (Å)	D (Å)
1380	310	3.568	2.199	0	1.90	0.30
β_B (10^{-8})	β_N (10^{-8})	n	c	d	h	
3.1448	1.9655	0.72751	38049	4.3484	-0.57058	

For testing reliability of the potential the h-BN elastic properties were estimated. The C_{11} constant agrees well with reference for bulk h-BN[4] ($C_{11}^{ref} = 750\ GPa, C_{11}^{theory} = 763\ GPa$).

In the simulation, the hemisphere of the mutually-static atoms (imitating the AFM tip) strained the BN membrane with fixed edges up to failure, with indentation increments of 0.02 Å. At each step system was relaxed using conjugated gradient minimization. The obtained dependence of strain energy *E* of BN sheet upon the deflection was fitted by the integrated eq. (2) :

$$E(\delta) = \sigma^{2D}(\pi a)\left(\frac{\delta^2}{2a}\right) + E^{2D}\left(q^3 a\right)\left(\frac{\delta^4}{4a^3}\right) + E_0,$$

from which the E^{2D} coefficient was obtained. Here σ^{2D} is the pretension in the film, *a* is the radius of structure, E^{2D} is the elastic constant. δ is the deflection of the atom in the center point, *q*=1/(1.05-0.15*nu-0.16*nu^2)=0.99 is a dimensionless constant related to the Poisson ration of boron nitride (nu=0.211) [5].

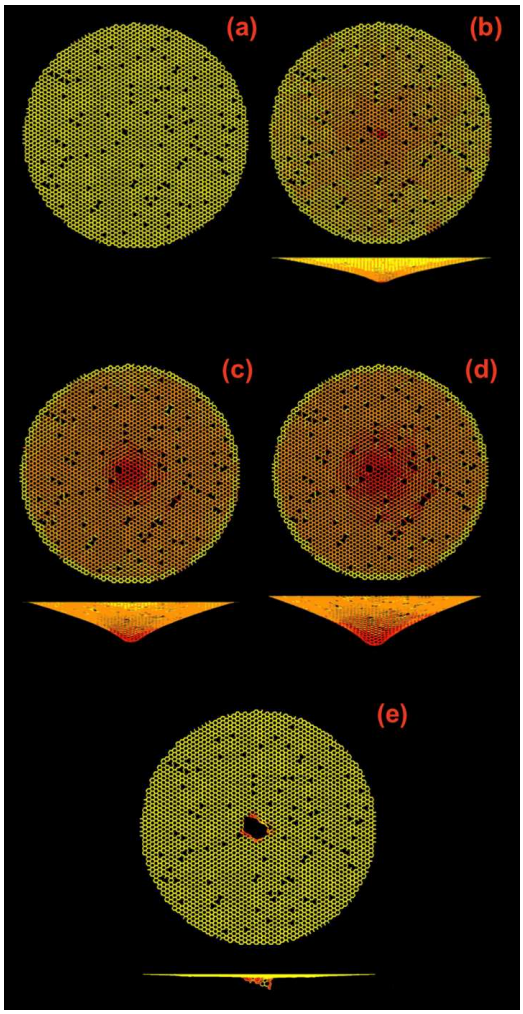

Fig. 4. Deformation process of BN membrane with 2% defects a) initial structure, b) δ = 15 Å, c) δ = 25 Å, d) δ = 31 Å (critical strain) and e) the fractured state. The gradation of color of bond lengths varies from red (1.61 – 1.75 Å) to yellow (1.44 – 1.46Å).

Reference:

1. Ci, L., Song, L.; Jin, C., Jariwala, D.; Wu, D.; Li. Y.; Srivastava, A.; Wang, Z.F.; Storr, K.; Balicas, L.; Liu, F.; Ajayan, P.M. Atomic layers of hybridized boron nitride and graphene domains. *Nature Materials* **2010**, 9, 430-435.

2. Tersoff, J. Modeling solid-state chemistry: Interatomic potentials for multicomponent systems. *Phys. Rev. B* **1989**, *39*, 5566-5568.

3. Verma, V.; Jindal, V K.; Dharamvir, K. Elastic modules of a boron nitride nanotube. *Nanotechnology* **2007,** *18*, 435711.

4. Duclaux, L.; Nysten, B.; Issi, J-P.; Moore, A.W. Structure and low-temperature thermal conductivity of pyrolytic boron nitride. *Phys. Rev. B* **1992**, *46*, 3362–3367.

5. Kudin, K.; Scuseria, G.; Yakobson, B. C_2F, BN, and C nanoshell elasticity from ab initio computations. *Phys. Rev. B* **2001**, *64*, 235406.